Natural Redundancy Resolution in Dual-Arm Manipulation using Configuration Dependent Stiffness (CDS) Control

Arash Ajoudani, Nikos G. Tsagarakis, Jinoh Lee, Marco Gabiccini and Antonio Bicchi

Abstract— Incorporation of human motor control principles in the motion control architectures for humanoid robots or assistive and prosthesis devices will permit these systems not only to look anthropomorphic and natural at the body ware level but also to generate natural motion profiles resembling those executed by humans during manipulation and locomotion. In this work, relying on the observations on human bimanual coordination, a novel realtime motion control strategy is proposed to regulate the desired Cartesian stiffness profile during the execution of bimanual tasks. The novelty of the proposed control scheme relies on the use of common mode stiffness (CMS) and configuration dependent stiffness (CDS) to regulate the size and directionality of the task space stiffness ellipsoid. Thanks to the CDS control, the proposed scheme is not only proved to be effective in regulating the desired stiffness ellipsoid but also permits to resolve the manipulator redundancy in a natural manner. The effectiveness of the controller is evaluated in an experimental setup in which two cooperating robotic arms are executing an assembly task. Experimental results demonstrate that the proposed dual-arm CDS-CMS controller is effective in tracking the desired stiffness ellipsoids as well as in producing human-like natural motions for the two robotic arms.

I. INTRODUCTION

In recent years, the fast growing interest in versatility and flexibility of robotic systems working closely and interacting with humans in co-operative tasks or acting as assisting or prosthesis systems had led to the development of a wide range of systems: from full body humanoid robot co-workers to anthropomorphic manipulator prosthesis and exoskeleton systems aiming to aid and improve the life of humans with special needs. Apart from resembling the human body in terms of kinematics and physical appearance, and to increase their acceptability and compatibility, such systems should be also capable of generating motions that look natural and demonstrate similarities with those executed by humans. To achieve this, it is profitable therefore to incorporate in the motion control architecture of these systems human principles of motor control [1].

The goal is to obtain a good performance, while rendering a human-like natural motion, which is deemed to emerge as a consequence of the stabilization of some task-related criteria. To illustrate the underlying concept, examples of natural postures of the human while holding a cup or using
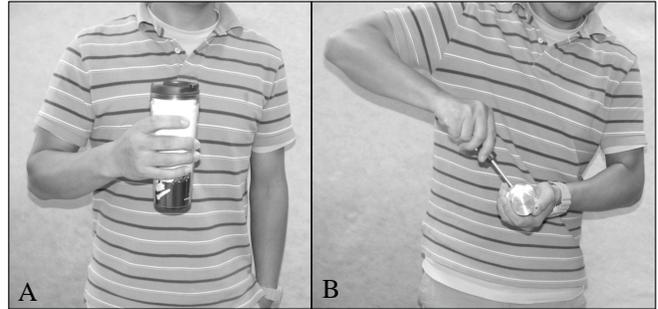
Arash Ajoudani, Marco Gabiccini and Antonio Bicchi are with Interdepartmental Research Centre "E. Piaggio", Faculty of Engineering, University of Pisa, and with the Dept. of Advanced Robotics, Istituto Italiano di Tecnologia, Via Morego 30, 16163, Genova, Italy (e-mails: arash.ajoudani@iit.it, m.gabiccini@ing.unipi.it and bicchi@centropiaggio.unipi.it).

Jinoh Lee and Nikos G. Tsagarakis are with the Dept. of Advanced Robotics, Istituto Italiano di Tecnologia, Via Morego 30, 16163, Genova, Italy (e-mail: {jinoh.lee, nikos.tsagarakis}@iit.it).

Fig. 1: Examples of acquired natural postures in humans as a consequence to the redundancy resolution for (A) minimum effort and (B) impedance control.

a screwdriver are depicted in Fig. 1. A and B, respectively. In these particular examples, subtask criteria are rooted in the concepts of minimum effort (1. A) and impedance control (1. B), which lead to the generation of corresponding configurations. Inspired by similar observations, the problem of redundancy resolution has been extensively addressed in the field of robotics by establishing task-related artificial potential fields [2], [3], [4], while, only few studies have drawn attention to the acquired human-like natural motion [5], [1], [6].

With the advent of higher demands on dual-arm manipulation, interaction with the environment using impedance control [7] became the focus of many studies in dual-arm systems. In this direction, object-level impedance control of cooperating robots has gained great attention due to the feasibility of controlling task forces/velocities while avoiding the occurrence of high internal forces [8]. In [9], an internal force based impedance controller has been proposed and its effectiveness was evaluated in an assembly task in a planar setup. Following that, Bonitz et al. [10] extended the aforementioned concept to a condition in which the dynamics of the object is not known. In [11], a decentralized impedance controller is proposed and its contact efficiency is evaluated in an industrial setup, in which two cooperating manipulators carry a common object. The authors in [12], [8] have presented object-level impedance controllers with coupling stiffness which is defined by a potential function. Even though such well-established techniques have successfully demonstrated their effectiveness through reliable handling of the contact, only few have highlighted the efficiency of the Cartesian impedance control through redundancy resolution [13], [14].

In this paper, relying on the major contribution of the arm configuration to effectively regulate the directionality of the realized endpoint stiffness ellipsoid, and its low-cost nature [15], [16], [17], we explore the role of *configuration dependent stiffness* (CDS) control [18], for dual-arm object manipulation. Therefore, the joint variables are controlled in redundant space to realize a task-specific Cartesian stiffness profile. In addition, with the purpose of obtaining a good tracking performance while rendering natural movements, we incorporate the optimality principles in human motor control in the development of proposed impedance controller. In this direction, given the growing body of evidence in support of coordinated stiffening behavior of the arm joints in humans (e.g. see [19], [15], [16]), we utilize the concept of *common mode stiffness* (CMS) control. To establish this concept, we assume a correlated stiffening behavior among the joints of each robot. A realtime optimization technique is then proposed to adjust the CMS and CDS variables and realize a desired Cartesian stiffness profile of the tool, w.r.t the object: While the CMS variations contribute to the modifications of the size of the realized stiffness ellipsoid (analogous to the role of co-contractions in human arm), CDS control will orient the realized stiffness ellipsoid toward the desired Cartesian profile.

The effectiveness of the proposed controller is evaluated in a dual-arm assembly task. The acquired good tracking performance and similarities between the natural postures of the human operators and the ones realized by the robots illustrate the contact efficiency of the proposed algorithm, while highlighting the advantages of the integration of human motor principles in redundancy resolution of dual-arm manipulation. Therefore, utilization of similar motion control strategies in humanoids co-operating with humans or upper limb assistive exoskeleton or prosthesis devices can result in the generation of more natural motions improving the acceptability and compatibility of such devices.

The rest of the paper is structured as follows; section II describes the development of the proposed controller. The experimental setup and results of the implementation of the controller for a dual-arm assembly task are presented in sections III and IV, respectively. Finally, section V addresses the conclusions.

II. CONTROLLER DESIGN

A. Dual-arm kinematics

Observations on human bimanual coordination suggest that the central nervous system (CNS) stabilizes the first synergy of the two cooperating arms to a larger degree (higher control levels) than if it did for control of each arm joints, separately. Indeed, as regards the human dual-arm activities in its most natural way, two hands cooperate in a way that they form a kinematic chain [20]: while the first synergy stabilizes the relative position/orientation of the two hands (as a dominant task requirement), lower hierarchical levels of control stabilize remaining task variables by controlling the redundant degrees of freedom [21], [22]. Above observations promote the idea of utilizing a similar kinematic
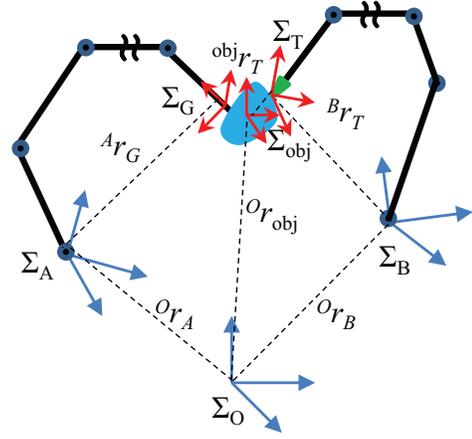

Fig. 2: Dual arm manipulation diagram.

representation in dual-arm robotic manipulation of the object to accommodate the stabilization of the task variables as well as rendering a natural redundancy resolution.

To that end, in our setup, a relative Jacobian is used which creates a unified, coordinated control between the two arms. Normally, the expression of the relative Jacobian combines the individual Jacobians of each arm, such that the resulting Jacobian maps the joint velocities of the two arms to the relative velocity between the end-effectors [23]. This allows users to directly specify the relative trajectory between the two end-effectors such that coordinating the trajectories of the two arms becomes an easy task. Such representation have been incorporated with force-guided control [24] and impedance control [25] as well.

The dual-arm manipulation setup is shown in figure (2). In our setup, $q_G \in \mathbb{R}^{n_A}$ and $q_T \in \mathbb{R}^{n_B}$ denote the joint variables of the manipulators A and B, respectively. Here, we assume that manipulator A is rigidly holding the object, while manipulator B is executing the defined task with the tool. The position vectors of the origins of gripper frame (Σ_G) and the tool frame (Σ_T) with respect to the base frames of the two manipulators (Σ_A and Σ_B) are denoted as $^A r_G$ and $^B r_T$, respectively. In addition, the position vectors of the origins of the tool and the object frame with respect to Σ_A and Σ_B are denoted as $^{\text{obj}} r_T$ and $^{\text{obj}} r_G$, respectively. According to [23], the transformation of the joint velocities $\dot{q} = [\dot{q}_G^T \ \dot{q}_T^T]^T \in \mathbb{R}^n$, onto the task space linear and angular velocities $v = [^{\text{obj}} \dot{r}_T \ ^{\text{obj}} \omega_T]^T \in \mathbb{R}^6$ is performed by the relative Jacobian, J_R, as follows

$$v = J_R(q)\dot{q}, \tag{1}$$

with $n = n_A + n_B$, where n_A and n_B denote the number of DoFs of the two manipulators.

B. Impedance control of dual-arm

To establish the mapping between the forces acting on the tool, $^{\text{obj}} F_T$, referenced from the object frame, and the required joint torques, τ, we can exploit the principle of

virtual work. Therefore, we can write

$$\Delta W_\tau = \tau^T \Delta q,$$
$$\Delta W_F = {}^{\text{obj}}F_T{}^T \Delta^{\text{obj}}x_T.$$

(2)

with ΔW_τ and ΔW_F, denoting the work done by the joint torques and displacements, and forces acting on the object and relative displacement of the tool w.r.t. object frame of reference, $\Delta^{\text{obj}}x_T$, respectively. By combining the Eqs. (1) and (2), we acquire

$$\tau = J_R^T(q) \ {}^{\text{obj}}F_T = J_R^T(q) \ K_c \ \Delta^{\text{obj}}\tilde{x}_T.$$

with $\Delta^{\text{obj}}\tilde{x}_T = {}^{\text{obj}}x_{Td} - {}^{\text{obj}}x_T$. On the other hand, to establish the stiffness mapping between the joint and Cartesian spaces, we employ the following expression [26],

$$K_J = \frac{\partial \tau}{\partial q} = \frac{\partial (J_R^T(q) \ K_c \ \Delta^{\text{obj}}\tilde{x}_T)}{\partial q},$$

The above equation can be written as follows, around the equilibrium position,

$$K_c = [J_R(q)(K_J - K_g)^{-1} J_R(q)^T]^{-1},$$

(3)

where the diagonal elements of the joint stiffness matrix $K_J \in \mathbb{R}^{n \times n}$ are formed by the diagonal elements of the joint stiffness matrices of the two robots (K_{J_G} and K_{J_T}). Here, we assume that all joint stiffness matrices do not have coupling terms, i.e. they are always of diagonal shape. The stiffness matrix K_c specifies the Cartesian stiffness profile which is defined with respect to Σ_G, and $K_g = \frac{\partial J_R^T(q)}{\partial q} \ {}^{\text{obj}}F_T \in \mathbb{R}^{n \times n}$, captures the effect of geometry in presence of external forces.

A very interesting outcome of the above relation is the definition of the desired Cartesian stiffness (the Cartesian stiffness between Σ_T and Σ_{obj})[1] in relative coordinates. This means that the need for transferring the configuration-dependent, desired Cartesian stiffness matrices of the two robots with respect to the world frame to the task coordinates is simplified, thanks to the definition of the relative Jacobian. Such realization will be profitable for dual-arm asymmetric manipulation tasks using tools (e.g. carving, peeling, peg-in-hole, etc) [20], since the specification of the task parameters in relative coordinates is more intuitive.

C. CMS and CDS Optimization Algorithm

To realize the desired Cartesian stiffness matrix (by tracking 21 elements in the symmetric matrix K_{cd}), in absence of preload forces (i.e. $K_g = 0$), we differentiate the Eq. 3 w.r.t. time as follows[2]:

$$\dot{K}_c = -K_c \left[\frac{dJ_R(q)}{dt} K_J^{-1} J_R(q)^T + J_R(q) \frac{d(K_J^{-1})}{dt} J_R(q)^T \right.$$
$$\left. + J_R(q) K_J^{-1} \frac{dJ_R(q)^T}{dt} \right] K_c,$$

(4)

with the first and the last terms of the above equation being the transpose of each other. To that end, if we take

[1]since Σ_G is considered rigidly attached to Σ_{obj}, the components of the stiffness matrix are expressed in Σ_{obj}.

[2]By taking into account that for a square and invertible matrix X, $\partial X^{-1} = -X^{-1}(\partial X)X^{-1}$.

into account that $\dot{q}$ is allowed to vary in the null-space of the relative Jacobian, while complying with the prescribed relative motion of the two end-effectors, we can write

$$\dot{q} = J_R^+ \upsilon + N_J \dot{\gamma},$$

(5)

where J_R^+ denotes the pseudo-inverse of the relative Jacobian, $\frac{dJ_R}{dt} = \frac{dJ_R}{dq} \dot{q}$, and $N_J \in \mathbb{R}^{n \times n-6}$ is a basis of the nullspace projector $(I - J_R^+ J_R)$ of the relative Jacobian. $\dot{\gamma} \in \mathbb{R}^{n-6}$ is the vector of nullspace velocities, and $I \in \mathbb{R}^n$ is the identity matrix. Now, by combining Eqs. (5) and (4), and defining

$$P_1 = \frac{dJ_R(q)}{dq} [J_R^+ \upsilon] K_J^{-1} J_R(q)^T$$
$$P_2 = \frac{dJ_R(q)}{dq} [N_J \dot{\gamma}] K_J^{-1} J_R(q)^T$$
$$P_3 = J_R(q) \frac{d(K_J^{-1})}{dt} J_R(q)^T$$
$$= J_R(q) \dot{K}_J^{-1} J_R(q)^T,$$

we can write

$$\dot{K}_c = -K_c[P_1 + P_2 + P_3 + P_1^T + P_2^T]K_c.$$

(6)

Now, if we decompose the nullspace velocity vector, we can write

$$\dot{\gamma} = \begin{bmatrix} 1 \\ \bar{0}_{n-7} \end{bmatrix} \dot{\gamma}_1 + \cdots + \begin{bmatrix} \bar{0}_{n-7} \\ 1 \end{bmatrix} \dot{\gamma}_{n-6},$$
$$= I_{\gamma_1} \dot{\gamma}_1 + \cdots + I_{\gamma_{n-6}} \dot{\gamma}_{n-6}.$$

(7)

Here, relying on the observations on coordinated stiffening behavior of the arm joints in humans (e.g. see [19], [15], [16]), we explore the concept of common mode stiffness introduced in [18], in our dual-arm setup. Therefore, we assume that the joint stiffness values are controlled in a coordinated manner. To replicate similar behavior, we choose a constant diagonal scaling matrix, K_{scales}, (in descending order from base joint to the end-effector [27]) for each arm while introducing two independently controlled common mode stiffness values, k_{cms_1} and k_{cms_2}. Therefore we write:

$$\dot{K}_J = K_{\text{scales}_1} \dot{k}_{cms_1} + K_{\text{scales}_2} \dot{k}_{cms_2}.$$

(8)

By combining Eqs. (6), (7) and (8), while factoring w.r.t. the scalar nullspace velocities, $\dot{\gamma}_i$, and common mode stiffness changes, $\dot{k}_{cms_i}$, we define

$$J_{\gamma_i} = \text{vec}\{\frac{dJ_R(q)}{dq}[N_J I_{k_{J_i}}]J_R(q)^T + \sim^T\}\dot{\gamma}_i$$
$$J_{K_{cms_i}} = \text{vec}\{-J_R(q)K_J^{-1}K_{\text{scales}_i}K_J^{-1}J_R(q)^T + \sim^T\}\dot{k}_{cms_i}$$

where the operator vec extracts the 21 independent elements of 6×6 symmetric matrix, and the symbol $\sim$ denotes the same term, placed in the same set of brackets. Now, by defining $\dot{\tilde{K}}_c = \dot{K}_c + K_c[P_1 + P_1^T]K_c$, we can write

$$\text{vec}\{\dot{\tilde{K}}_c\} = \begin{bmatrix} J_\gamma & J_{K_{cms}} \end{bmatrix} \begin{bmatrix} \dot{\gamma} \\ \dot{k}_{cms} \end{bmatrix} =: J_y \dot{y}.$$

(9)

with $J_\gamma = [J_{\gamma_1} \cdots J_{\gamma_{n-6}}]$, $J_{K_{cms}} = [J_{K_{cms_1}} \ J_{K_{cms_2}}]$, $\dot{\gamma} = [\dot{\gamma}_1 \cdots \dot{\gamma}_{n-6}]^T$, and $\dot{k}_{cms} = [\dot{k}_{cms_1} \ \dot{k}_{cms_2}]^T$.

The above equation resembles the structure of inverse kinematics problem, in which we are dealing with the tracking of $\dot{\bar{K}}_c \in \mathbb{R}^{21}$ by using common mode stiffness values, k_{cms}, and degrees of kinematic redundancy in a dual-arm setup. Now, by defining the vectorial stiffness error $e_s = \text{vec}\{K_{cd} - K_c\}$, we can set up classical update laws. Consequently, by exploiting the update law based on the pseudo-inverse of J_y we get

$$\dot{y} = J_y^+ \left[\text{vec}\{\dot{\bar{K}}_c\} + K_{ps} e_s \right], \tag{10}$$

where K_{ps} is the gain associated to the stiffness error e_s. Eq. 10 synchronously updates the CMS (k_{cms}) and CDS (γ) values through corresponding Jacobians, $J_{K_{cms}}$ and J_γ, respectively. Therefore, iterative optimization of the CMS and CDS values will result in the realization of a desired Cartesian stiffness profile in realtime. In the meantime, the desired motion of the tool w.r.t. the gripper frame of reference will be assured due to the Eq. 5.

D. Task Prioritization

To execute a dual-arm manipulation task, the object must be held in a reasonable position, inside the workspace, w.r.t. the world frame of reference. This is accompanied by the desired relative motion of the tool w.r.t. the object frame, and cost-efficient motion of the remaining degrees of freedom in dual-arm kinematic chain. Therefore, the task can be decomposed into subtasks with prioritized order of occurrence.

An efficient solution for stabilization of the task variables in prioritized order is presented in [4]. Following that, to preserve a desired position of the object w.r.t. the world frame, the first priority subtask is established as follow

$$\dot{q}_G = J_1^+ \dot{r}_1, \tag{11}$$

where $J_1 \in \mathbb{R}^{3 \times n_A}$ is the first-priority task Jacobian and $\dot{r}_1 \in \mathbb{R}^3$ is the velocity vector of the origin of the gripper frame[3]. Our secondary subtask establishes the relative movement of the two end effectors and its kinematic relationship is defined by the relative Jacobian of the two cooperative manipulators (Eq. 1). Now, given the two subtasks, we setup the task-priority based kinematic control [4], as follows[4]

$$\dot{q} = J_1^+ \dot{r}_1 + \hat{J}_2^+ (\dot{r}_2 - J_2 J_1^+ \dot{r}_1) + (I - J_1^+ J_1)(I - \hat{J}_2^+ \hat{J}_2)\dot{\gamma}, \tag{12}$$

where I is the identity matrix, $J_2 = J_R$, $\dot{r}_2 = \upsilon$, and $\hat{J}_2 = J_2(I - J_2^+ J_2)$. To ensure robustness against kinematic singularities, we use the damped least squares inverse solution which is defined by $B^+ = B^T(BB^T + \lambda I)^{-1}$, with $\lambda \in \mathbb{R}$ denoting the damping factor [28].

The third term in above equation projects the vector $\dot{\gamma}$ (Eq. 9), into a subspace ($C \in \mathbb{R}^{n-9}$, assuming $n > 9$) which is formed by remaining DoF that do not affect neither one of the subtask variables, while, at the same time decreases the error between the desired and realized relative stiffness profile.

---

[3]here we do not consider any constraints on the orientation of the first subtask.

[4]such representation accommodates the incorporation of additional subtasks such as joint and torque limit avoidance and etc.
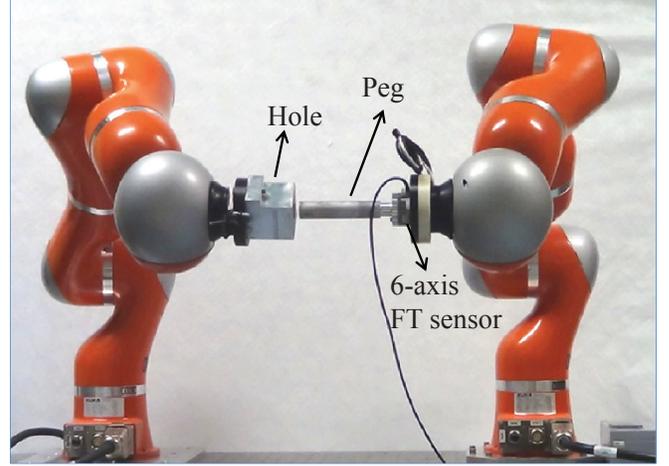

Fig. 3: Dual-Arm assembly (peg-in-hole) setup.

Due to the fact that the proposed algorithm incorporates human impedance regulation principles in realization of the desired Cartesian stiffness profile, we expect to obtain similar performance and natural redundancy resolution as compared with the humans.

The proposed CDS controller can also be utilized for humanoid robots or upper body assistive devices with joints with fixed-passive stiffness values to fairly realize a desired Cartesian stiffness profile w.r.t. the object frame. In addition, once the concept of common mode stiffness is integrated in the hardware[5], the CDS controller can be adopted to further reduce the error between the realized and desired Cartesian stiffness profiles.

III. EXPERIMENTAL SETUP

The efficiency of the proposed approach to cope with contact stability issues while generating natural motions in redundant space is evaluated in a Peg-in-Hole task, a classical benchmark for spatial planning with uncertainties.

The dual-arm setup incorporated two seven DoF KUKA LWR, with DLR's Fast Research (FR) Interface [29]. A peg and a hole were designed and mounted on the end effectors of the two robots. To illustrate the capabilities of the proposed controller in effective modulations of the size and directionality of the realized endpoint stiffness in task coordinates, the hole was mounted along different (x, y and z) directions of Σ_G. Then, three different desired Cartesian, $K_{c_{des}}$, stiffness profiles (stiff along the direction of the hole, while realizing a compliant profile along other directions to avoid generation of high interaction forces) were defined and tracked by our proposed controller. The task-required value of the desired Cartesian stiffness matrix along the hole axis (in which there is friction) was chosen from the human endpoint stiffness measurements [19]. A 6–axis force and

---

[5]by designing robotic arms with $n+1$ actuators, with n being the number of joints and 1 corresponding the actuator for modifying the stiffness of all joints in a coordinated manner.
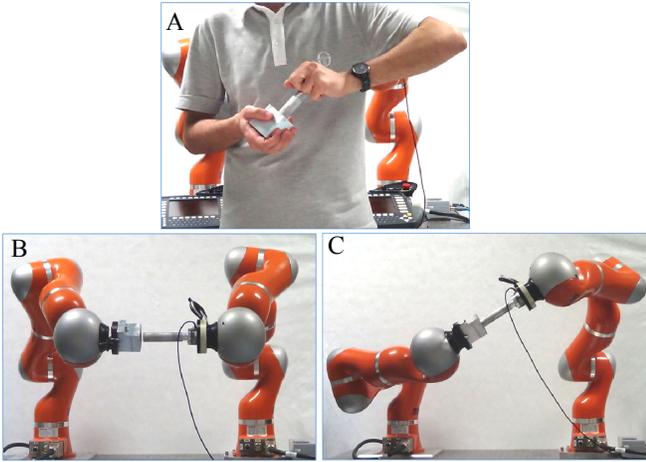
Fig. 4: A. Human performing a bimanual peg-in-hole task. Initial configuration (B), and realized configuration as a result of proposed controller (C). Human and robots' ending configuration coincide which gives evidence to the similarity in control principles.

torque (F/T) sensor (ATIMini-45) was mounted in between the peg and the robot end effector to monitor the interaction forces. Performance analysis of the proposed algorithm was carried out considering the realized stiffness matrix error and normalized to the norm of $K_{c_{des}}$ as follows

$$e_K = \frac{\|K_c - K_{c_{des}}\|}{\|K_{c_{des}}\|}.$$

In addition, to provide a graphical representation of the stiffness profiles, the translational part of the realized and desired stiffness matrices were projected into xy, xz and yz planes of the object frame of reference, Σ_{obj}, resulting in three stiffness matrices ($K_{ij} \in \mathbb{R}^2, [i, j] = [x, y, z]$). Following that, the major, α_{max}, and minor, α_{min}, axis of the ellipsoids along with the major axis direction, φ_{ij}, were determined using singular value decomposition:

$$\varphi_{ij} = \text{atan2}(U_{\text{max}_j}, U_{\text{max}_i})$$
$$\alpha_{max_{ij}} = [\text{E}_{\text{max}}(K_{ij}^T K_{ij})]^{\frac{1}{2}}$$
$$\alpha_{min_{ij}} = [\text{E}_{\text{min}}(K_{ij}^T K_{ij})]^{\frac{1}{2}},$$

with E denoting the eigenvalue operator and $K_{ij} = U_{ij}S_{ij}V_{ij}^T$.

The joint damping values were all considered fixed $D_i = 0.7\text{Ns/m}$. The control and synchronization interface between the KUKA controllers and the six axis F/T sensor were developed in C++.

IV. RESULTS

Figure 4. A demonstrates the natural posture of the human operator executing an assembly task. As observed here, the redundant DoFs in both arms are adapted to orient the stiffness profile in the direction of the hole, to overcome the frictional forces, while rendering a compliant behavior in remaining directions to avoid generation of high interaction forces.
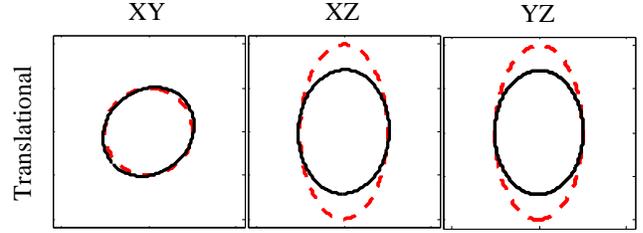

Fig. 5: Desired (red, dashed) and realized (black, solid) translational stiffness ellipsoids, corresponding to configuration C in Fig. 4. In this experiment, the translational stiffness matrix $K_{c_{des}} = [300, 300, 1000]$N/m, is defined in relative coordinates. All off diagonal elements are set to zero. The hole is mounted along the z axis of Σ_G.
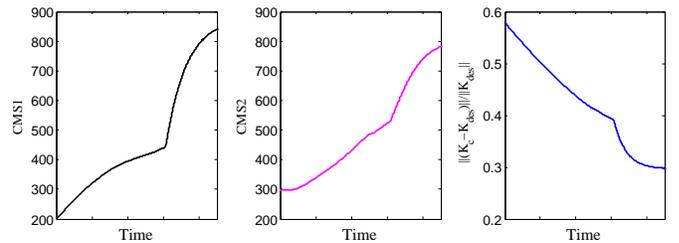

Fig. 6: Common mode stiffness parameters of the two robots (left and middle plots) are adapted in addition to the CDS to decrease the error between the desired and realized stiffness ellipsoids (most right plot), in realtime. The error at the begging of the experiment can be though of a case in which only CMS optimization was taken into account. While, synchronous optimization of the CMS and CDS parameters results in an effective reduction in the stiffness error profile

The proposed algorithm establishes the realtime tracking of the desired stiffness profile in relative coordinates through the optimization of the CMS and CDS. Starting from an initial configuration (Fig. 4. B), the CDS control drives the redundant joints to a configuration which is depicted in Fig. 4. C.

The desired (red, dashed) and realized (black, solid) ellipsoids are projected into the object's frame of reference and are depicted in Fig. 5. As seen in the plots, efficient elongation of the stiffness ellipsoid is perceived due to the CDS control. Fig. 6 illustrates the adaptation of the CMS values of the two robots (most left and middle plots), synchronized with CDS control of the dual-arm setup. The error (Fig. 6, most right plot) at the begging of the experiment can be though of a case in which only CMS parameters' optimization was taken into account. While, synchronous optimization of the CMS and CDS parameters result in effective reduction in the stiffness error profile.

In another experiment, the hole was mounted along the y axis of Σ_G and the desired stiffness ellipsoid was defined to render a stiff behavior along the direction of the hole, while being compliant along other directions. Starting from an initial configuration depicted in Fig. 7. B, the
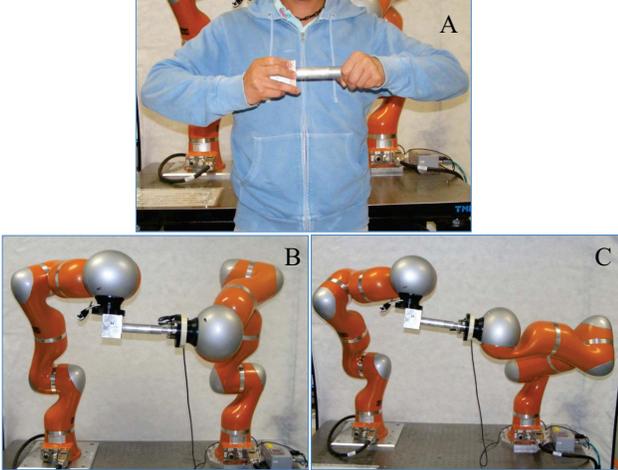
Fig. 9: Desired (red, dashed) and realized (black, solid) translational stiffness ellipsoids with different elongation w.r.t. Fig. 5. In this experiment, the translational stiffness matrix $K_{c_{des}} = [1000, 300, 300]$N/m, is defined in relative coordinates. All off diagonal elements are set to zero.

red stiffness ellipsoid in relative coordinates (the hole was mounted along x in this experiment). The CDS and CMS values are adapted to effectively align the realized stiffness ellipsoid with the desired one. This lead to the normalized error of $e_K = 30\%$.

Effective modulations of the size and the directionality of the realized stiffness ellipsoid in above examples illustrate the capabilities of the proposed controller in realization of the desired Cartesian stiffness profile. In addition, our proposed CDS controller achieves a natural redundancy resolution of the dual-arm setup, which highlights its application in control of the humanoids or upper body assistive or prosthesis devices.

V. CONCLUSIONS

The paper proposed a new on-line motion controller which regulates the Cartesian stiffness ellipsoid in a manner inspired by human motor control and impedance regulation principles. The presented scheme not only achieves effective task space stiffness control but also intrinsically perform redundancy resolution of the manipulator arm in a manner that results in the generation of natural motion resembling those executed by human in similar tasks. In particular, relying on the observations on coordinated stiffening behavior of the human arm joints, two common mode stiffness (CMS) controllers were utilized. The CMS concept was introduces in our dual arm controller by changing the joint stiffness values of each robotic arm in a correlated manner. This allows to regulate the size of the realized Cartesian stiffness ellipsoid for each arm. Simultaneously, to align the realized stiffness ellipsoid with the desired one, we explored the concept of configuration dependent stiffness (CDS) in dual arm impedance control. Effectiveness of the proposed algorithm in efficient modifications of the realized size and directionality of the task stiffness ellipsoid, while generating natural movements, was evaluated in three assembly experiments. Implementation of the CMS-CDS controller resulted in good tracking performance, in addition to the generation of natural movements, similar to the ones realized by human operators.

It is worth to point out that, here, the naturalness of the robot motions were mainly determined based on the visual

Fig. 7: A. Human performing a bimanual peg-in-hole task. Initial configuration (B), and realized configuration as a result of proposed controller (C). The hole was kept in a fixed position (subtask one), while the orientation was allowed to change due to the CDS. Human and robots' ending configuration coincide which gives evidence to the similarity in control principles.
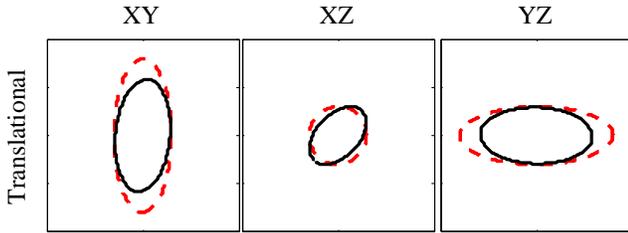

Fig. 8: Desired (red, dashed) and realized (black, solid) translational stiffness ellipsoids, corresponding to configuration C in Fig. 4. In this experiment, the translational stiffness matrix $K_{c_{des}} = [300, 1000, 300]$N/m, is defined in relative coordinates. All off diagonal elements are set to zero. The hole is mounted along the Y axis of Σ_G.

CDS control drives the redundant joints to a configuration which is depicted in Fig. 7. C. Since the position of the hole is considered fixed, the CDS controller has maximally adjusted the configuration of the manipulator on the left, not to violate the constraints on the position of the hole. At the same time, efficient control of the configuration of the manipulator on the right has been achieved. Similarities between the natural posture of the human operator (Fig. 7. A), and the one realized by the proposed controller, once again, give evidence to the analogy between incorporated control principles. The normalize error between the realized and desired task stiffness profile was $e_K = 27\%$. This error includes all 21 elements of the stiffness matrices. Projected stiffness ellipsoids of this experiment are brought in Fig. 8.

Fig. 9 illustrates the projected stiffness ellipsoids, as results of the tracking of different elongation of the desi-
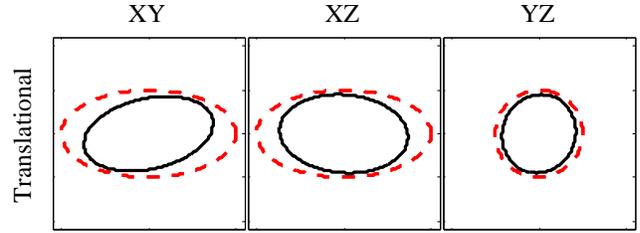
comparison with human postures making similar tasks as the ones commanded to the robot. Future works will be devoted to the establishment of more solid metrics to measure the naturalness of the robot motions and compare them to a "non natural" redundancy resolution.

VI. ACKNOWLEDGMENTS

REFERENCES

[1] O. Khatib, E. Demircan, V. De Sapio, L. Sentis, T. Besier, and S. Delp, "Robotics-based synthesis of human motion," *Journal of Physiology-Paris*, vol. 103, no. 3, pp. 211–219, 2009.

[2] B. Cao, G. I. Dodds, and G. W. Irwin, "Redundancy resolution and obstacle avoidance for cooperative industrial robots," *Journal of Robotic Systems*, vol. 16, no. 7, pp. 405–417, 1999.

[3] H. Seraji, "Task options for redundancy resolution using configuration control," in *Decision and Control, 1991., Proceedings of the 30th IEEE Conference on*. IEEE, 1991, pp. 2793–2798.

[4] Y. Nakamura, *Advanced robotics: redundancy and optimization*. Addison-Wesley Longman Publishing Co., Inc., 1990.

[5] D. Matsui, T. Minato, K. F. MacDorman, and H. Ishiguro, "Generating natural motion in an android by mapping human motion," in *IEEE/RSJ International Conference on Intelligent Robots and Systems, IROS 2005*. IEEE, 2005, pp. 3301–3308.

[6] A. M. Zanchettin, P. Rocco, L. Bascetta, I. Symeonidis, and S. Peldschus, "Kinematic analysis and synthesis of the human arm motion during a manipulation task," in *IEEE International Conference on Robotics and Automation (ICRA), 2011*, pp. 2692–2697.

[7] C. Ott, *Cartesian impedance control of redundant and flexible-joint robots*. Springer, 2008, vol. 49.

[8] T. Wimböck, C. Ott, A. Albu-Schäffer, and G. Hirzinger, "Comparison of object-level grasp controllers for dynamic dexterous manipulation," *The International Journal of Robotics Research*, vol. 31, no. 1, pp. 3–23, 2012.

[9] S. Schneider and R. Cannon Jr, "Object impedance control for cooperative manipulation: Theory and experimental results," *IEEE Transactions on Robotics and Automation*, vol. 8, no. 3, pp. 383–394, 1992.

[10] R. Bonitz and T. Hsia, "Internal force-based impedance control for cooperating manipulators," *IEEE Transactions on Robotics and Automation*, vol. 12, no. 1, pp. 78–89, 1996.

[11] F. Caccavale, P. Chiacchio, A. Marino, and L. Villani, "Six-dof impedance control of dual-arm cooperative manipulators," *IEEE/ASME Transactions on Mechatronics*, vol. 13, no. 5, pp. 576–586, 2008.

[12] A. Dietrich, T. , and A. Albu-Schaffer, "Dynamic whole-body mobile manipulation with a torque controlled humanoid robot via impedance control laws," in *Proceedings of 2011 IEEE/RSJ International Conference on Intelligent Robots and Systems (IROS)*, Sept. 2011, pp. 3199–3206.

[13] A. Albu-Schaffer, M. Fischer, G. Schreiber, F. Schoeppe, and G. Hirzinger, "Soft robotics: what cartesian stiffness can obtain with passively compliant, uncoupled joints?" in *IEEE/RSJ International Conference on Intelligent Robots and Systems, 2004.*, vol. 4. IEEE, 2004, pp. 3295–3301.

[14] W. Owen, E. Croft, and B. Benhabib, "Acceleration and torque redistribution for a dual-manipulator system," *Robotics, IEEE Transactions on*, vol. 21, no. 6, pp. 1226–1230, 2005.

[15] R. Trumbower, M. Krutky, B. Yang, and E. Perreault, "Use of self-selected postures to regulate multijoint stiffness during unconstrained tasks," *PLoS One*, vol. 4, no. 5, 2009.

[16] T. Milner, "Contribution of geometry and joint stiffness to mechanical stability of the human arm," *Experimental Brain Research*, vol. 143, pp. 515–519, 2002.

[17] E. Perreault, R. Kirsch, and P. Crago, "Voluntary control of static endpoint stiffness during force regulation tasks," *Journal of Neurophysiology*, vol. 87, pp. 2808–2816, 2002.

[18] A. Ajoudani, M. Gabiccini, N. G. Tsagarakis, A. Albu-Schäffer, and A. Bicchi, "TeleImpedance: Exploring the role of common-mode and configuration-dependant stiffness," in *IEEE International Conference on Humanoid Robots*, 2012.

[19] A. Ajoudani, N. G. Tsagarakis, and A. Bicchi, "Tele-Impedance: Teleoperation with impedance regulation using a body-machine interface," *International Journal of Robotics Research*, vol. 31(13), pp. 1642–1655, 2012, http://www.youtube.com/watch?v=KPO6IO7Tr-Q.

[20] Y. Guiard, "Asymmetric division of labor in human skilled bimanual action: The kinematic chain as a model," *Journal of motor behavior*, vol. 19, pp. 486–517, 1987.

[21] K. Hinckley, R. Pausch, D. Proffitt, J. Patten, and N. Kassell, "Cooperative bimanual action," in *Proceedings of the ACM SIGCHI Conference on Human factors in computing systems*. ACM, 1997, pp. 27–34.

[22] Y. Guiard, "The kinematic chain as a model for human asymmetrical bimanual cooperation," *Advances in Psychology*, vol. 55, pp. 205–228, 1988.

[23] A. Mohri, M. Yamamoto, and G. Hirano, "Cooperative path planning for two manipulators," in *Robotics and Automation, 1996. Proceedings., 1996 IEEE International Conference on*, vol. 3. IEEE, 1996, pp. 2853–2858.

[24] J.-D. Choi, S. Kang, M. Kim, C. Lee, and J.-B. Song, "Two-arm cooperative assembly using force-guided control with adaptive accommodation," in *IEEE/RSJ International Conference o Intelligent Robots and Systems, 1999.*, vol. 2, 1999, pp. 1253–1258.

[25] J. Lee, P. Chang, and R. Jamisola, "Relative impedance control for dual-arm robots performing asymmetric bimanual tasks," *IEEE Transactions on Industrial Electronics*, 2013, in press.

[26] S.-F. Chen and I. Kao, "Conservative congruence transformation for joint and cartesian stiffness matrices of robotic hands and fingers," *The International Journal of Robotics Research*, vol. 19, no. 9, pp. 835–847, 2000.

[27] H. Gomi and M. Kawato, "Human arm stiffness and equilibrium-point trajectory during multi-joint movement," *Biological cybernetics*, vol. 76, no. 3, pp. 163–171, 1997.

[28] S. Chiaverini, "Singularity-robust task-priority redundancy resolution for real-time kinematic control of robot manipulators," *Robotics and Automation, IEEE Transactions on*, vol. 13, no. 3, pp. 398–410, 1997.

[29] G. Schreiber, A. Stemmer, and R. Bischoff, "The fast research interface for the kuka lightweight robot," in *IEEE Conference on Robotics and Automation (ICRA)*, 2010.